

REPORT DOCUMENTATION PAGE

Form Approved OMB NO. 0704-0188

The public reporting burden for this collection of information is estimated to average 1 hour per response, including the time for reviewing instructions, searching existing data sources, gathering and maintaining the data needed, and completing and reviewing the collection of information. Send comments regarding this burden estimate or any other aspect of this collection of information, including suggestions for reducing this burden, to Washington Headquarters Services, Directorate for Information Operations and Reports, 1215 Jefferson Davis Highway, Suite 1204, Arlington VA, 22202-4302. Respondents should be aware that notwithstanding any other provision of law, no person shall be subject to any penalty for failing to comply with a collection of information if it does not display a currently valid OMB control number.

PLEASE DO NOT RETURN YOUR FORM TO THE ABOVE ADDRESS.

1. REPORT DATE (DD-MM-YYYY)	2. REPORT TYPE New Reprint	3. DATES COVERED (From - To) -		
4. TITLE AND SUBTITLE Ammonia Vapor Removal by Cu3(BTC)2 and Its Characterization by MAS NMR		5a. CONTRACT NUMBER W911NF-07-1-0053		
		5b. GRANT NUMBER		
		5c. PROGRAM ELEMENT NUMBER BD2256		
6. AUTHORS Gregory W. Peterson, George W. Wagner, Alex Balboa, John Mahle, Tara Sewell, Christopher J. Karwacki		5d. PROJECT NUMBER		
		5e. TASK NUMBER		
		5f. WORK UNIT NUMBER		
7. PERFORMING ORGANIZATION NAMES AND ADDRESSES New York Structural Biology RRL 317B 1275 York Ave. New York, NY 10021 -6094		8. PERFORMING ORGANIZATION REPORT NUMBER		
9. SPONSORING/MONITORING AGENCY NAME(S) AND ADDRESS(ES) U.S. Army Research Office P.O. Box 12211 Research Triangle Park, NC 27709-2211		10. SPONSOR/MONITOR'S ACRONYM(S) ARO		
		11. SPONSOR/MONITOR'S REPORT NUMBER(S) 51980-CH.5		
12. DISTRIBUTION AVAILABILITY STATEMENT Approved for public release; distribution is unlimited.				
13. SUPPLEMENTARY NOTES The views, opinions and/or findings contained in this report are those of the author(s) and should not be construed as an official Department of the Army position, policy or decision, unless so designated by other documentation.				
14. ABSTRACT Adsorption equilibria and NMR experiments were performed to study the adsorption and interactions of ammonia with metal-organic framework HKUST-1, or Cu3(BTC)2 (BTC) 1,3,5-benzenetricarboxylate). Ammonia capacities determined from chemical breakthrough measurements show significantly higher uptake capacities than from adsorption alone, suggesting a stronger interaction involving a potential reaction with the Cu3(BTC)2 framework. Indeed, 1H MAS NMR reveals that a major disruption of the relatively simple spectrum of				
15. SUBJECT TERMS metal-organic frameworks, Cu3(BTC)2, HKUST-1, 1H MAS NMR, 13C MAS NMR,				
16. SECURITY CLASSIFICATION OF: a. REPORT UU		17. LIMITATION OF ABSTRACT UU	15. NUMBER OF PAGES	19a. NAME OF RESPONSIBLE PERSON Michael Goger
				19b. TELEPHONE NUMBER 212-939-0660

Report Title

Ammonia Vapor Removal by Cu3(BTC)2 and Its Characterization by MAS NMR

ABSTRACT

Adsorption equilibria and NMR experiments were performed to study the adsorption and interactions of ammonia with metal-organic framework HKUST-1, or Cu3(BTC)2 (BTC) 1,3,5-benzenetricarboxylate).

Ammonia capacities determined from chemical breakthrough measurements show significantly higher uptake capacities than from adsorption alone, suggesting a stronger interaction involving a potential reaction with the Cu3(BTC)2 framework. Indeed, ^1H MAS NMR reveals that a major disruption of the relatively simple spectrum of Cu3(BTC)2 occurs to generate a composite spectrum consistent with Cu(OH)2 and (NH4)3BTC species under humid conditions the anticipated products of a copper(II) carboxylate reacted with limited ammonia. These species are not detected under dry conditions; however, reaction stoichiometry combined with XRD results suggests the partial formation of an indeterminate diammine copper(II) complex with some residual Cu3(BTC)2 structure retained. Cu(II)-induced paramagnetic shifts exhibited by various species in ^1H and ^{13}C MAS NMR spectra are consistent with model compounds and previous literature. Although results show extensive ammonia capacity of Cu3(BTC)2, much of the capacity is due to reaction with the structure itself, causing a permanent loss in porosity and structural integrity.

REPORT DOCUMENTATION PAGE (SF298)
(Continuation Sheet)

Continuation for Block 13

ARO Report Number 51980.5-CH
Ammonia Vapor Removal by Cu₃(BTC)₂ and Its ...

Block 13: Supplementary Note

© 2009 . Published in The Journal of Physical Chemistry C, Vol. 113 (31) (2009), (31). DoD Components reserve a royalty-free, nonexclusive and irrevocable right to reproduce, publish, or otherwise use the work for Federal purposes, and to authorize others to do so (DODGARS §32.36). The views, opinions and/or findings contained in this report are those of the author(s) and should not be construed as an official Department of the Army position, policy or decision, unless so designated by other documentation.

Approved for public release; distribution is unlimited.

Ammonia Vapor Removal by Cu₃(BTC)₂ and Its Characterization by MAS NMR

Gregory W. Peterson,* George W. Wagner, Alex Balboa, John Mahle, Tara Sewell, and Christopher J. Karwacki

Edgewood Chemical Biological Center, 5183 Blackhawk Rd., APG, Maryland 21010-5424

Received: March 26, 2009; Revised Manuscript Received: June 12, 2009

Adsorption equilibria and NMR experiments were performed to study the adsorption and interactions of ammonia with metal–organic framework HKUST-1, or Cu₃(BTC)₂ (BTC = 1,3,5-benzenetricarboxylate). Ammonia capacities determined from chemical breakthrough measurements show significantly higher uptake capacities than from adsorption alone, suggesting a stronger interaction involving a potential reaction with the Cu₃(BTC)₂ framework. Indeed, ¹H MAS NMR reveals that a major disruption of the relatively simple spectrum of Cu₃(BTC)₂ occurs to generate a composite spectrum consistent with Cu(OH)₂ and (NH₄)₃BTC species under humid conditions—the anticipated products of a copper(II) carboxylate reacted with limited ammonia. These species are not detected under dry conditions; however, reaction stoichiometry combined with XRD results suggests the partial formation of an indeterminate diammine copper(II) complex with some residual Cu₃(BTC)₂ structure retained. Cu(II)-induced paramagnetic shifts exhibited by various species in ¹H and ¹³C MAS NMR spectra are consistent with model compounds and previous literature. Although results show extensive ammonia capacity of Cu₃(BTC)₂, much of the capacity is due to reaction with the structure itself, causing a permanent loss in porosity and structural integrity.

Introduction

Highly porous structures possessing functionalized active sites are essential for retention of light vapors. Permanent adsorption of ammonia presents a unique challenge due to its high vapor pressure and reversibility as a weakly bound ligand. Although a number of adsorbent materials, such as activated carbons impregnated with copper chloride, have been shown to be effective during the initial uptake of ammonia, the adsorption affinities are sufficiently low such that ammonia desorption results from ambient temperature purge.^{1,2} Because the commercially available adsorbents such as activated carbons and zeolites exhibit ammonia off-gassing even at low (10^{-5}) relative pressures or are ineffectual in the presence of humidity, more active sorbents are sought to reduce the volume of filtration systems. Of particular note are metal–organic frameworks (MOFs) or porous-coordination polymers (PCPs).

MOFs represent a relatively new class of porous materials that can be tailored to modify surface area, pore size, functionality, and topology through reticular chemistry,^{3–6} a methodology advanced by Yaghi and co-workers. Reticular chemistry permits the synthesis of predetermined structures by utilizing a variety of inorganic and organic building blocks, thus allowing the development of high capacity materials customized for specific removal chemistries. Although the majority of work on MOFs to date has focused on gas storage applications,^{7–10} this class of materials shows promise for a broad range of air purification applications. Reticular chemistry permits the synthesis of predetermined structures by utilizing a variety of inorganic and organic building blocks, thus allowing the development of high capacity materials customized for specific removal chemistries.

Although MOFs have been studied for over a decade, very limited data exist on dynamic removal of toxic gases in air

SCHEME 1: Generic Amide Formation



purification applications.^{11–13} Yaghi and co-workers¹¹ studied dynamic breakthrough of six MOFs against several toxic chemicals and found that pore structure and functionality played important roles in toxic gas removal. Lercher and co-workers^{12,13} similarly studied the dynamic removal of SO_x by Cu-BTC analogues, and reported the oxidation of SO_x by impregnated Cu-BTC. Chui and co-workers¹⁴ evaluated HKUST-1, or Cu₃(BTC)₂, for ammonia removal from contaminated air streams. Cu₃(BTC)₂ is formed by paddlewheel secondary building units (SBUs) containing Cu²⁺ dimers coordinatively linked to carboxylic oxygen atoms from organic benzene-1,3,5-tricarboxylate (BTC) ligands.^{14,15} Previous studies have shown that, once formed, the copper atoms in Cu₃(BTC)₂ are unsaturated^{14,15} and may therefore be available for chemisorption with ammonia, which is known to form coordination complexes with alkali and transition metals.^{1,16–18}

The reaction of ammonia with the individual building blocks of Cu₃(BTC)₂, i.e., Cu(II) ion and BTC, is well known. In aqueous solution, Cu(II) ion, in the presence of limited ammonia, is initially converted to Cu(OH)₂; however, copious amounts of ammonia eventually yield [Cu(NH₃)₄]²⁺.¹⁹ Carboxylic acids initially form the ammonium salt (Scheme 1) which, with sufficient heating, can be pyrolyzed to their corresponding amides:²⁰

It is further noteworthy, in particular, that copper salts of aromatic acids (i.e., Cu₃(BTC)₂) are known to react with ammonia (with heating) to generate aromatic amines,²⁰ a reaction involving scission of the copper–carboxylate ionic bond.

Other studies conducted on gas sorption behavior of Cu₃(BTC)₂, as well as other open-metal site MOFs, concluded that the unsaturated metal sites may contribute significantly to gas uptake.^{21–23} Furthermore, the relatively weak acidic coor-

* To whom correspondence should be addressed. E-mail: gregory.w.peterson@us.army.mil. Phone: (410) 436-9794. Fax: (410) 436-5513.

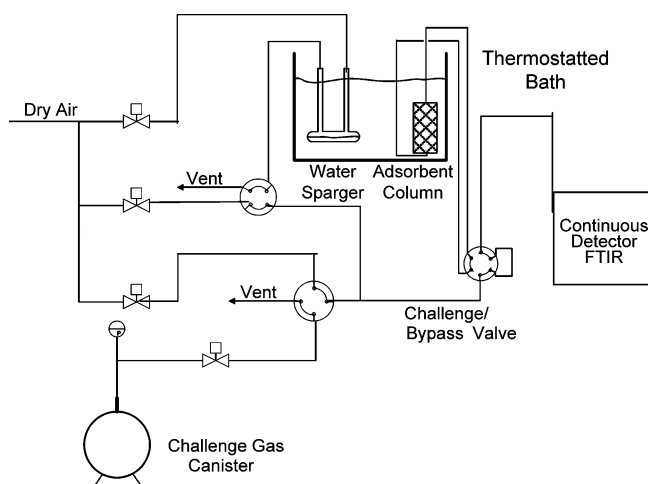


Figure 1. Microbreakthrough system schematic.

dination bonds of the structure may provide additional reactive centers for ammonia removal. In this work we present a detailed study of the ammonia removal properties of Cu₃(BTC)₂ through breakthrough analysis, nitrogen isotherm data, PXRD, and MAS NMR.

Experimental Section

Materials. Cu(acetate)₂(H₂O), Cu(L-tartrate)₃(H₂O)₃, Cu(CO₃)₂·Cu(OH)₂, 1,3,5-benzenetricarboxylic acid, NH₄HCO₃, and *N,N*-dimethylformamide (DMF) were obtained from Aldrich Chemical Co. and used without further purification.

Cu₃(BTC)₂ Synthesis. Cu₃(BTC)₂ was synthesized by Yaghi's group at UCLA.²⁴ Briefly, Cu₃(BTC)₂ was synthesized by stirring benzene-1,3,5-tricarboxylic acid and copper nitrate in a solvent consisting of DMF, ethanol, and deionized water. The reaction was allowed to proceed for ~24 h at a temperature of 85 °C and subsequently immersed in dichloromethane for 3 days. The crystals were activated under high vacuum at a temperature of 170 °C.

Nitrogen Adsorption Equilibria. Nitrogen adsorption equilibria on clean and ammonia-exposed Cu₃(BTC)₂ were measured on a Quantachrome Autosorb-1. Each sample of Cu₃(BTC)₂ was exposed to a relative pressures ranging from 10⁻⁵ to a maximum pressure of 1 atm. Adsorbed volumes were initially reported at STP and subsequently converted to equivalent liquid volumes at the boiling point of nitrogen. Pretreatment conditions for the unexposed and ammonia-exposed Cu₃(BTC)₂ were 150 °C for 16 h under vacuum (~1 × 10⁻⁹ atm).

Ammonia Breakthrough. A microscale breakthrough apparatus was developed to assess the adsorption and reaction behavior of adsorbent samples for air purification applications. The system was designed to operate at near ambient temperature over a range of humidities. A schematic of the test apparatus is presented in Figure 1. The test conditions are summarized in Table 1. Briefly, the system utilizes a small adsorbent sample size (~5–10 mg) packed into a nominal 4 mm i.d. fritted glass tube. The chemical is delivered as a dilute gas stream using a gas sampling canister which has been purged with dry air and sealed. A measured volume of ammonia is injected into the canister through a septum using a gastight syringe which is subsequently pressurized to 1 atm. The contents were delivered by a calibrated mass flow controller and verified with a bubble meter. The dry chemical stream was mixed with either a dry or humid air dilution stream to achieve a concentration of 1000 mg/m³ at the either dry (~40 °C dew point) or humid (80%

TABLE 1: Microbreakthrough Operating Conditions for Evaluation of Cu₃(BTC)₂

operating condition	value
temperature	20 °C
relative humidity	~40 °C (~0%) dew point and 80%
adsorbent mass	5–10 mg
adsorbent volume	55 mm ³
flow rate	20 mL/min
airflow velocity	2.7 cm/s
residence time	0.16 s

relative humidity), and challenged to Cu₃(BTC)₂ samples at a flow rate of 20 sccm (referenced to 20 °C). The effluent stream was continuously monitored for ammonia and water breakthrough to saturation with an FTIR (Nicolet 380, with DTGS detector).

A Cu₃(BTC)₂ sample was loaded into the sample tube and dried at 100 °C in a nitrogen stream. The sample tube was then conditioned under dry or humid conditions. The ammonia challenge was then conducted until saturation and followed by then purged with a clean stream. Following the purge step, the once-exposed samples were removed and dried at 100 °C under nitrogen. A second breakthrough test was then performed at the same conditions of the first exposure with ammonia. Results of the second exposure would confirm irreversible ammonia effects.

PXRD. X-ray scattering patterns were obtained using a Bruker D8 Discover X-ray diffractometer in the locked-coupled (θ – θ) mode with monochromated Cu K α (1.54 Å) radiation (40 kV, 40 mA) and scanned between $2\theta = 1^\circ$ and 50° with a step size (170.6 s/step) of $2\theta = 0.021013^\circ$. Additional X-ray scattering patterns were obtained using a Siemens D5005 X-ray diffractometer in the locked-coupled (θ – θ) mode with Cu K α (1.54 Å) radiation (40 kV, 40 mA) monochromated using a Gobel mirror and a thin film detector. Samples were mounted on a quartz low-background sample holder (limiting the characterization to shallow depth to avoid background signals) and scanned between $2\theta = 5^\circ$ and 120° with a step size (2 s/step) of $2\theta = 0.02^\circ$.

Cu₃(BTC)₂ Reactions. Cu₃(BTC)₂–NH₄HCO₃ Reaction. Cu₃(BTC)₂ (18.3 mg, 30.2 μmol) was added to 1 mL of D₂O containing 186 mg of NH₄HCO₃ (2.4 mmol) with stirring. An immediate, clear, dark-blue solution formed. ¹H NMR spectra of the solution showed dissolved BTC (8.77 ppm) and DMF (8.29, 3.37, and 3.22 ppm), yielding an apparent mole ratio of 0.32 DMF per BTC. Thus, the Cu₃(BTC)₂ contained 7.5 wt % residual DMF.

BTC–NH₄HCO₃ Reaction. BTC (500 mg, 2.4 mmol) was dry-mixed with 600 mg of NH₄HCO₃ (7.6 mmol) to which 0.5 mL of H₂O was added with stirring. Immediate gas evolution indicated the desired reaction was occurring, and it subsided after several minutes. The resulting material was allowed to dry in air to recover the solid (NH₄)₃BTC. ¹³C CP-MAS NMR confirmed the identity and purity of the trisubstituted material.

BTC–Cu(CO₃)₂–Cu(OH)₂–NH₄HCO₃ Reaction. BTC (100 mg, 480 μmol), 160 mg of Cu(CO₃)₂·Cu(OH)₂ (720 μmol), and 400 mg of NH₄HCO₃ (5.1 mmol) were stirred in 1 mL of H₂O. Immediate gas evolution resulted and the solution turned dark blue. After being stirred overnight, the dark-blue solution was allowed to dry in air to yield a dark-blue solid.

NMR. ¹H MAS NMR spectra were obtained using 30–45° pulses and relaxation delays of 1–2 s on Varian Unityplus 300WB, INOVA 400WB and 600NB, and Bruker AVANCE 750WB NMR spectrometers equipped with Doty Scientific 7-mm Super Sonic (300WB and 400WB) and 5-mm XC (600NB and 750WB) VT-MAS NMR probes. ¹³C MAS NMR

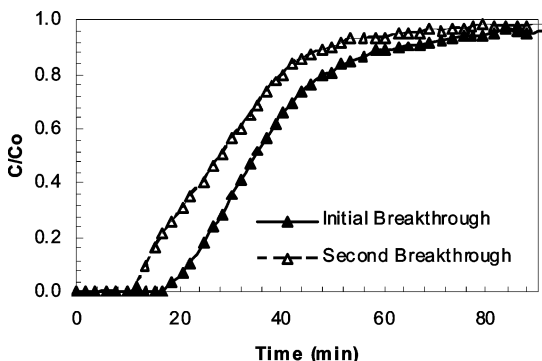


Figure 2. Ammonia breakthrough of $\text{Cu}_3(\text{BTC})_2$ in dry air.

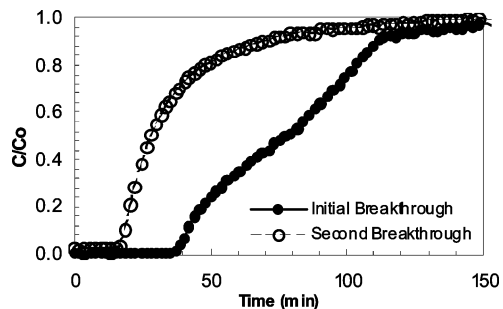


Figure 3. Ammonia breakthrough of $\text{Cu}_3(\text{BTC})_2$ at 80% relative humidity.

TABLE 2: NH₃ Capacities of Cu₃(BTC)₂ Samples

Cu ₃ (BTC) ₂ sample	capacity (mol/kg)	capacity (mol/mol Cu ₃ (BTC) ₂)
dry/first exposure	6.6	4.0
dry/second exposure	2.8	1.7
humid/first exposure	8.9	5.4
humid/second exposure	1.0	0.6

spectra were obtained at 100.6 MHz on the Varian 400WB instrument and, for Cu_3BTC_2 , direct excitation (90° pulses) and relaxation delays of 1–2 s was employed (cross-polarization “CP” was not used). ¹³C CP was used for the $(\text{NH}_4)_3\text{BTC}$ model compound (see below) using a 5 ms contact time and a relaxation delay of 2 s. Solution NMR spectra were obtained on the Varian Unityplus 300WB NMR spectrometer using a standard 5-mm solution NMR probe. All spectra were referenced to external TMS.

Results and Discussion

Ammonia Breakthrough Capacity. Ammonia breakthrough experiments for once- and twice-exposed $\text{Cu}_3(\text{BTC})_2$ samples were conducted. In the breakthrough curves, Figures 2–3, the twice-exposed samples exhibit a significantly reduced ammonia capacity relative to the once exposed samples. Ammonia is known to be able to complex with either the copper atoms or the carboxylates of the MOF framework. The performance of the once- and twice-exposed $\text{Cu}_3(\text{BTC})_2$ samples under both dry and humid conditions are summarized in Table 2. Integration of the breakthrough curve to saturation is used to calculate the dosage (concentration–time product, C_t) and capacity (retained ammonia mass per mass of $\text{Cu}_3(\text{BTC})_2$). Note that substantial loss in capacity is exhibited by the twice exposed samples.

The shape of the first and second exposure breakthrough curves under dry conditions are similar, while those at humid conditions differ. The dry case indicates that thermal regeneration does result in partially restored adsorption capacity. The

humid case first exposure suggests a slight discontinuity at ~50% of the feed concentration, perhaps a result of significant change in the structure of the $\text{Cu}_3(\text{BTC})_2$. The humid second exposure sample shows rapid breakthrough consistent with loss of porosity.

The reaction under dry conditions indicates 4 mol NH_3 per mol of $\text{Cu}_3(\text{BTC})_2$ are sequestered. Thus, in the absence of water, the formation of a diammine–copper species is implicated which would allow up to six NH_3 if the reaction were to go to completion prior to ammonia breakthrough. Such a species, $\text{Cu}(\text{NH}_3)_2\text{CO}_3$, is known,²⁵ and the compound undergoes slow decomposition upon exposure to moist air, apparently to $\text{Cu}(\text{OH})_2\text{Cu}(\text{CO}_3)$. Scheme 2 shows the formation of the analogous compound for $\text{Cu}_3(\text{BTC})_2$, “ $\text{Cu}(\text{NH}_3)_2\text{BTC}_{2/3}$ ”, under dry conditions, the carboxylates of BTC serving as the counterion ligands rather than carbonate to form this indeterminate species. The moisture-promoted decomposition of the diammine species is also shown, forming an indeterminate copper-hydroxide, the slight formation of which is detected by ¹H MAS NMR (see below).

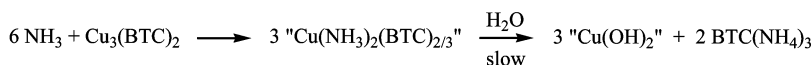
With ample water, ammonium salts of the BTC might be anticipated to form (see Scheme 1) with concomitant formation of $\text{Cu}(\text{OH})_2$. Thus, this first reaction, shown in Scheme 2, accounts for up to six NH_3 . The capacity for NH_3 observed under humid conditions is consistent with Scheme 2, although it might be postulated that some NH_3 is solubilized by sorbed water or by the (limited) formation of tetraammine copper species which, as discussed in the Introduction, are known to form by the action of NH_3 on $\text{Cu}(\text{OH})_2$ in aqueous solutions (Scheme 2). These proposed reactions for the dry and humid samples are consistent with ¹H MAS NMR characterizations (see below). In particular, ¹H MAS NMR (see below) detects a major species attributable to $\text{Cu}(\text{OH})_2$ for the humid sample but only slight formation of this species in the dry sample.

For the samples exposed a second time, the residual observed capacity for NH_3 can arise from (1) incomplete conversion during the first exposure (only 4.0 and 5.4 mol out of the possible 6 NH_3 per mol of Cu_3BTC_2 , respectively, are taken up by the dry and humid samples), (2) the formation of additional tetraammine copper(II) in the case of the humid material, and/or (3) some thermal decomposition of the di- and tetraamminenocuppper(II) complexes during activation to release their sequestered NH_3 as shown at the bottom of Scheme 2. Note that in the case of the dry sample “ Cu_3BTC_2 ” is not the original structure, just the indeterminate material remaining following loss of the NH_3 . For the dry sample, the presence of its greater residual capacity (1.7 mol of NH_3 per mol of Cu_3BTC_2) compared to that of the humid sample (0.6) could be simply due to residual, unreacted material (detected by XRD). The ammonium carboxylate species formed in the humid sample are apparently extremely stable salts, which would not be expected to release NH_3 during activation to regenerate the free carboxylate; rather, as discussed above, ammonium is retained by carboxylates during heating, eventually forming amides when heated to sufficiently high temperatures (Scheme 1)—a reaction that would not regenerate NH_3 capacity.

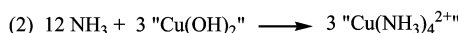
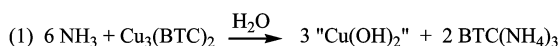
The reactions depicted in Scheme 2 obviously involve the structural collapse of the MOF, creating materials of indeterminate structure. This is supported by PXRD data, as shown in Figure 5, and ¹H MAS NMR (see below). It should be noted that, in the presence of water, the reaction presented in Scheme 2 for the humid condition can indeed proceed to completion as confirmed by the observation that stirring a water-suspension of $\text{Cu}_3(\text{BTC})_2$ with excess NH_4HCO_3 leads to its complete

SCHEME 2

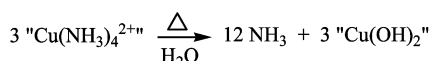
Dry Condition:



Humid Condition:



Activation of Spent Materials:



dissolution and an immediate deep blue color, characteristic of the expected [Cu(NH₃)₄(H₂O)₂]²⁺ complex (see Experimental Section).

Chiu¹⁴ has determined the Cu₃(BTC)₂ cubic symmetry with the space group designation of *Fm*³*m*. Using the deposited CIF file at the Cambridge Crystallographic Data Centre within the Cambridge Structural Database, one can use software such as Mercury to simulate the powder X-ray diffraction pattern. Comparing the simulated powder X-ray diffraction pattern with prepared Cu₃(BTC)₂ confirms the overall state of the starting materials prior to ammonia vapor exposure. In the case of Cu₃(BTC)₂ exposed to dry ammonia vapor, there is some clear indication that the Cu₃(BTC)₂ has lost some of its original crystallinity tending to a more amorphous material. The appearance of new peaks and disappearance of original peaks confirms the differences of crystal symmetry in the case of Cu₃(BTC)₂ exposed to humid ammonia vapor. Differences between different starting and humid ammonia vapor challenged Cu₃(BTC)₂ materials can be seen in the Supporting Information figures. A tabulation of the experimental and simulated PXRD peaks were compiled, but no rigorous indexing has been carried out to fully characterize these differences. It was noted that there were some subtle differences between the experimental and simulation that are difficult to explain at present.

Nitrogen Adsorption Equilibria on Ammonia Exposed Cu₃(BTC)₂. Nitrogen adsorption isotherm measurements at the boiling point of nitrogen, 77.34 K, were performed on

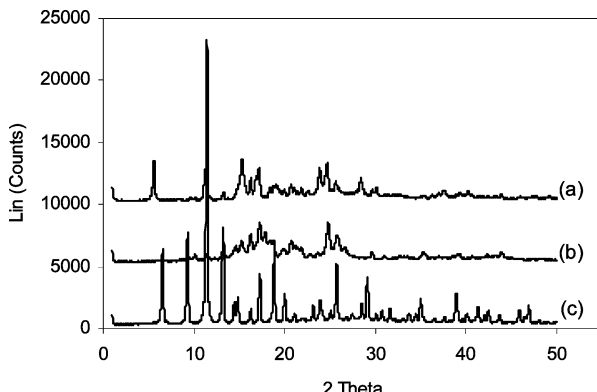


Figure 5. PXRD data indicate that the humid once ammonia exposed (a) sample has a significantly different XRD pattern than the unexposed sample (c), indicating a complete change in the Cu₃(BTC)₂ framework. The dry once-exposed (b) sample has a pattern somewhere in between the unexposed and once-exposed humid samples.

Cu₃(BTC)₂ before and after exposure to ammonia. Figure 6 shows a linear plot of the measured isotherm data, and Figure 7 shows a log plot of the same data with amplification of the nitrogen adsorbed volumes at relative pressures below 10⁻¹.

In Figure 6, data show that the ammonia-unexposed sample exhibits a classic type I isotherm with a small amount of hysteresis. A majority of the nitrogen is adsorbed at relative pressures less than 10⁻³. Molecular simulations of Ar adsorption isotherm data on similar Cu–BTC structures indicated that

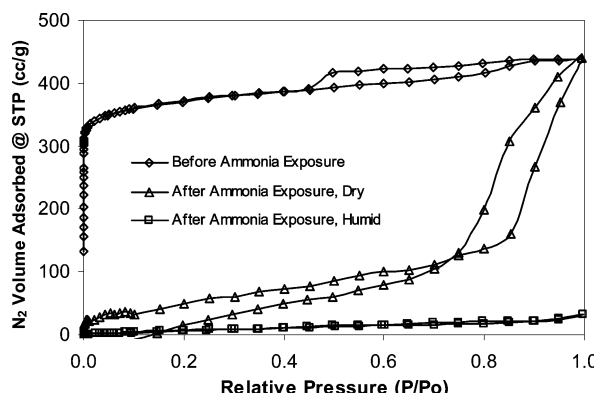


Figure 6. Nitrogen isotherms of Cu₃(BTC)₂ before and after ammonia exposure. The dry, once-exposed sample exhibits capillary filling, indicating the presence of some macroporosity; however, the humid, once-exposed sample has very limited nitrogen adsorption, indicating structural collapse and/or pore blockage.

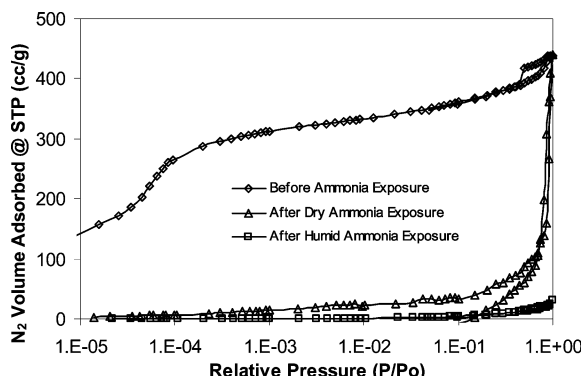


Figure 7. Log plot of nitrogen isotherms of Cu₃(BTC)₂ before and after ammonia exposure. Neither the dry, once-exposed nor humid, once-exposed samples show any low-level nitrogen adsorption, indicating the absence of micropores.

TABLE 3: Calculated Porosity and Apparent Surface Area Values from Nitrogen Adsorption Isotherm Data

$\text{Cu}_3(\text{BTC})_2$ sample	BET capacity (m^2/g)	total pore volume at STP (cc/g)	DR ^a micropore volume at STP (cc/g)
ammonia unexposed	1460	0.68	0.54
dry once-exposed	150	0.68	0.06
humid once-exposed	16.2	0.49	0.003

^a Dubinin–Radushkevich adsorption isotherm equation.

TABLE 4: Ammonia and Nitrogen Adsorption Capacity of $\text{Cu}_3(\text{BTC})_2$

$\text{Cu}_3(\text{BTC})_2$ sample	adsorbate	relative pressure	capacity ^a (cc/g-adsorbent)
dry unexposed	ammonia	0.000145	218.0 ^b
dry unexposed	nitrogen	0.000145	301 ^c
dry once-exposed	ammonia	0.000145	106.5
dry once-exposed	nitrogen	0.000145	0.20

^a Capacity at $P/P_s = 0.000145$, equivalent to 1000 mg/m³ (1.093 mmHg) NH₃, $P_{\text{sat}} = 7500.0$ mmHg at 298 K, $V_m(\text{NH}_3) = 24.78$ L/mol at 298 K. ^b Ammonia capacity at 298 K determined from breakthrough measurements (see Table 2). ^c Nitrogen volume adsorbed corrected to 298 K. See Supporting Information, Figure S1.

preferential adsorption exists in the tetrahedron side pockets of the lattice,¹⁵ indicating strong interaction energies within the microporous substrate, likely created by the unsaturated copper atoms.

The hysteresis loop at relative pressures above 0.4 corresponds to previous argon adsorption studies by Vishnayakov and co-workers and is indicative of mesoporous defects formed during crystallization.¹⁵ The exhausted samples exposed to ammonia under dry and 80% RH conditions show a significant decrease in nitrogen adsorption at all relative pressures. Under these conditions, the exhausted sample exposed to ammonia at 80% RH has lost essentially all porosity. Figure 7 shows the same data as Figure 6 plotted on a logarithmic pressure scale. At low-to-mid relative pressures, the fresh Cu₃(BTC)₂ sample adsorb over 2 orders of magnitude more nitrogen than the exhausted samples. This is indicative of a loss of microporosity and is substantiated in the values calculated from the isotherm data.

Table 3 summarizes the BET capacity (or apparent surface area), the total pore volume, and the apparent micropore volume. The fresh material exhibits 10 times greater apparent surface area than the dry, ammonia once-exposed sample and 100 times greater apparent surface area than the humid, ammonia once-exposed sample. The apparent total pore volume is not greatly different between the three samples as this quantity is calculated at a high relative pressure, where all three samples show significant nitrogen adsorption. The apparent micropore volume indicate that the microporous channels of the fresh material have been greatly widened after exposure to both dry and humid ammonia challenges, further indicating that the porous network has rearranged.

Table 4 shows the measured capacities of the Cu₃(BTC)₂ for ammonia and nitrogen at a relative pressure equivalent to the ammonia feed concentration (1000 mg/m³, $P_i = 1.093$ mmHg, 298 K) used in the breakthrough experiments discussed above. The nitrogen capacity at 0.000145 relative pressure for the unexposed sample is higher than the ammonia capacity for the same sample by about 38%. Following exposure to ammonia, the nitrogen capacity decreases markedly to about 0.20 mL-

N₂/g-sorbent, indicating complete collapse of the structure and loss of microporosity.

On the basis of the NH₃ capacity, the N₂ isotherms are in good agreement for the capacity reduction associated with NH₃ adsorption and thermal regeneration.

NMR of Paramagnetic Compounds. For MAS NMR, Cu₃(BTC)₂ presents a challenge, owing to its paramagnetic Cu(II). Ishii et al.²⁶ have pointed out the difficulty of assigning peaks as a result of large paramagnetic shifts and that line-narrowing by high-power proton decoupling is not as effective due to the large spectral distribution of paramagnetic shifts. Moreover, McDermott et al.²⁷ noted that wide spinning sideband patterns arise which are reflective of the large paramagnetic shift dispersion, chemical shift anisotropy, and bulk susceptibility anisotropy.

Even still, McDermott et al.²⁷ point out that well-resolved MAS NMR spectra can be obtained in favorable cases where slow electron spin–lattice relaxation and electron spin-diffusion are effective at “decoupling” individual protons from the (normal) global proton dipolar-coupled spin system. In these instances carbon–proton pairs behave as isolated spin systems. Thus, when well-resolved ¹H MAS NMR spectra are observed, well-resolved ¹³C MAS NMR spectra are also obtained without the need for high-power proton decoupling as reasonable MAS spinning rates are sufficient to overcome residual C–H couplings within spin pairs.

For example, Ishii et al.,²⁶ in their ¹³C MAS NMR study of Cu(alanine)₂(H₂O) (Figure 8), noted problems with decoupling the rigid methine and carboxyl groups with conventional cw ¹H decoupling at modest spinning speeds ($\nu_R = 5$ kHz). However, they were still able to obtain good quality spectra using the ¹H self-decoupling provided by very fast MAS ($\nu_R = 24$ kHz) of the “paramagnetically-isolated” putative CH and CH₃ spin pairs. Further, peak assignments were possible based on ¹³C–¹H dephasing behavior, the effects of which were severe for CH (−269 ppm; rigid), moderate for CH₃ (173 ppm; rotating), and small for CO₂[−] (−183 ppm; rigid, but no directly attached protons). These assignments for Cu(alanine)₂(H₂O) are shown in Table 5. Thus, the observed strength of the ¹H–¹³C dipole interaction, whether diminished by distance or internal motion, was still valid for making assignments in this paramagnetic complex. Such considerations regarding residual dipolar interactions can similarly be employed to render ¹³C MAS NMR assignments for Cu₃(BTC)₂ and related model compounds (Figure 8) as discussed below.

¹H MAS NMR of Cu₃(BTC)₂. The most striking feature present in the ¹H MAS NMR spectrum of Cu₃(BTC)₂ (Figure 9) is the wide pattern of rather narrow spinning sidebands, indicative of a rigid species unencumbered by homonuclear dipolar effects. The central peak of the sideband pattern is at 8.1 ppm and is straightforwardly assigned to the ring protons of the BTC constituent. There are at least two other similarly sharp peaks which, lacking spinning sidebands, are obviously due to motionally averaged species. Improvement in resolution was obtained at higher field, Figure 9, where near-baseline resolution is achieved for the three major peaks at 750 MHz (17.5 T) along with slightly better resolution of smaller, overlapping peaks (see below).

The anhydrous form of Cu₃(BTC)₂ is purple, whereas the hydrated form is blue.²⁸ Exposing a nominally dry sample of Cu₃(BTC)₂ to air resulted in the series of spectra shown in Figure 10. It is clear from these spectra that adsorbed water yields the peak at ca. 12.6 ppm (H₂O…Cu), with all the peaks tending to shift upfield with increased water uptake. Further note that peaks

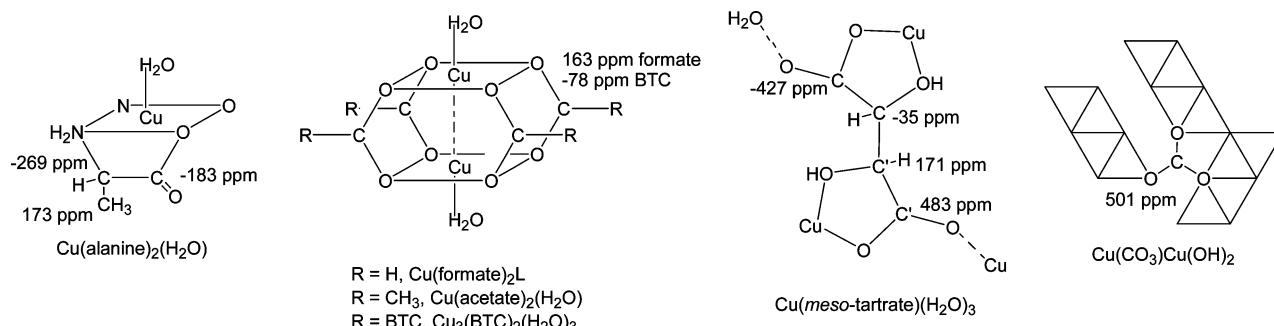


Figure 8. Succinct structural elements of Cu₃(BTC)₂ and Cu(II)-containing model compounds indicating ¹³C MAS NMR assignments. Assignments may be reversed for Cu(tartrate)(H₂O)₃ (see text). Although the structure for Cu(*meso*-tartrate)(H₂O)₃ is shown, Cu(*L*-tartrate)(H₂O)₃ (and presumably the *L*-tartrate model compound under study) similarly possesses the two types of CO₃²⁻ and HCOH groups which are differentiated by prime notation.²⁹ The binuclear Cu(formate)₂ core structure shown is stabilized in the presence of amine-type ligands but not water.³⁰ For Cu(CO₃)Cu(OH)₂ edge-sharing Cu(II) octahedral chains (two octahedrals wide) are represented by triangles, strips of which are linked³¹ by the CO₃²⁻ group as indicated.

TABLE 5: ¹³C and ¹H MAS NMR Shifts Observed for Cu₃(BTC)₂ and Model Compounds

compound	group	¹³ C (temp)	¹ H	ref
Cu(alanine)₂(H₂O)	CO ₂ ²⁻	−183 (331 K)	—	
	CH	−269 (331 K)	8.4 (298 K)	26 (¹³ C)
	CH ₃	173 (331 K)	28.1 (298 K)	27 (¹ H)
Cu(<i>L</i> -tartrate)(H ₂ O) ₃	NH ₂	—	−146 (298 K)	
	CO ₂ ²⁻ '	483 ^a (298 K)	—	
	CH'	171 ^b (298 K)	6 (298 K) ^b	this work
	CH	−35 ^b (298 K)	4 (298 K) ^b	
Cu(CO ₃)Cu(OH) ₂	CO ₂ ²⁻	−427 ^c (298 K)	—	
	CO ₃ ²⁻	501 (298 K)	—	this work
Cu(formate) ₂ (C ₅ H ₅ N)	HCO ₂ [−]	163 (92 K)	—	29
Cu(acetate) ₂ (H ₂ O)	CO ₂ ²⁻	no signals observed down to 173 K	—	
	CH ₃	—	15 (298 K)	this work
Cu ₃ (BTC) ₂ ·xDMF·yH ₂ O	CO ₂ ²⁻	−78 (298 K)	—	
	=CH−	228 (298 K)	8.1 (298 K)	
	=C<	240,218 (298 K)	—	this work
	H ₂ O	—	~12.7 (298 K) ^c	
	CH ₃ (DMF)	38 (298 K)	9.7, 7.1 (298 K)	
	HC=O (DMF)	165 (298 K)	ca. 12.7 (298 K) ^d	

^a CO₂²⁻ assignments may be reversed. ^b CH assignments may be reversed. ^c Peak shifts upfield with increasing water adsorption. ^d Underlies H₂O peak.

assigned to residual, adsorbed DMF (see below) are observed to be easily displaced/perturbed by water as previously noted by Chui et al.¹⁴ That adsorbed water shifts intensity from the downfield DMF peak to the upfield DMF peak is consistent with the assignment of these two peaks to DMF···Cu and DMF displaced to the channels, respectively (see below).

The identity of the remaining sharp ¹H MAS NMR peak(s) was inferred from ¹³C MAS NMR spectra (see below) which revealed that the sample of Cu₃(BTC)₂ contained a considerable amount of DMF, apparently left over from its synthesis.¹⁴ Heating a sample of Cu₃(BTC)₂ in air at 170–180 °C while intermittently observing the ¹H and ¹³C MAS NMR spectra (Figure 11, left side) revealed immediate loss of the residual water peak at 12.7 ppm, slower loss of peak intensity at 7.1 ppm, and even slower loss of peak intensity at 9.7 ppm. Loss of intensity for the latter two peaks correlated with loss of intensity for DMF in ¹³C MAS NMR spectra (not shown); thus, these two peaks are attributed to Cu(II)-bound DMF (9.7 ppm) and “channel-DMF”¹⁴ (7.1 ppm) as a result of their relative desorption propensities. Also, these assignments are consistent with the water-displacement behavior noted above.

Further confirmation of the assignments of these peaks to adsorbed DMF was obtained by observing changes in ¹H and ¹³C MAS NMR spectra after adding liquid DMF to the same

sample (right side of Figure 11). In initial spectra, a broad feature at 2.3 ppm was observed to quickly dissipate within minutes whereas a second peak at −6.0 ppm persisted for days, and these peaks are attributed to bulk DMF liquid and DMF sorbed on the (exterior) surface of the crystallites. The peaks of interest at 9.7 and 7.1 ppm remained unaltered while the sample sat at room temperature. Annealing the sample at 100 °C for 23 h apparently assisted readsorption of DMF; first into the channels (7.1 ppm) and eventually coming to rest at the Cu(II) sites (9.7 ppm). Exposure to air restores the intensity of the water peak at 12.7 ppm with concomitant sharpening of the DMF peaks, presumably due to increased motion afforded by the coadsorbed water. As further confirmation of these assignments, Soxhlet-extracted (MeOH) Cu₃(BTC)₂ is totally devoid of both DMF peaks, leaving only the pristine methine spinning sideband pattern and a residual water peak (see Supporting Information).

¹³C MAS NMR of Cu₃(BTC)₂. ¹³C MAS NMR spectra obtained for Cu₃(BTC)₂, with and without high-power proton decoupling, are shown in Figure 12 (the large peak near 115 ppm common to both spectra is due to the Kel-F rotor end-caps). The difference between the two spectra is startling: In the absence of decoupling, a sharp set of spinning sidebands is observed containing a center band at 228 ppm, whereas decoupling causes the sharp 228-ppm peak to vanish and the

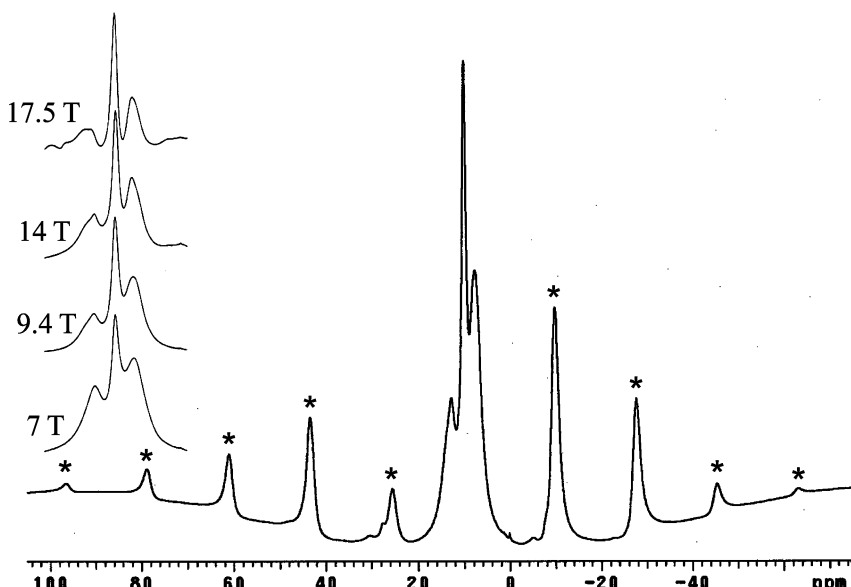


Figure 9. 400 MHz (9.4 T) ^1H MAS NMR spectra obtained for dry $\text{Cu}_3(\text{BTC})_2$. Inset shows resolution of centerbands achieved at 7, 9.4, 14, and 17.5 T. Spinning sidebands are marked by asterisks.

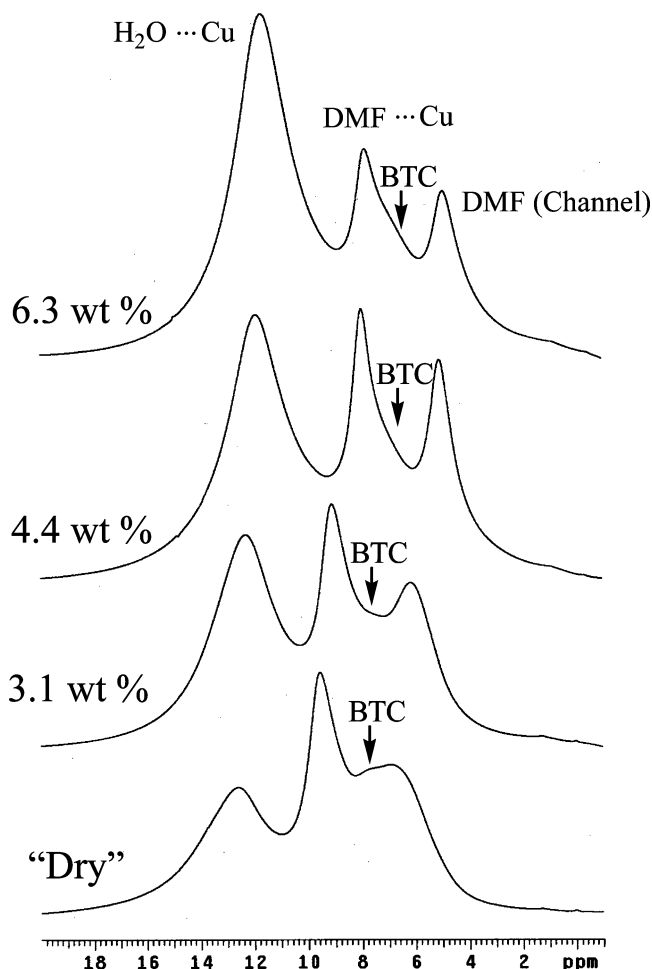


Figure 10. ^1H MAS NMR spectra (9.4 T) obtained for nominally dry $\text{Cu}_3(\text{BTC})_2$ before and after exposure to air for (bottom to top) 0, 2, 3.5, and 7 h. Percent weight gain is as indicated.

emergence of two broad peaks at 240 and 218 ppm along with their less-wide spinning sideband patterns. Such behavior is consistent with that observed by Ishii et al.²⁶ for $\text{Cu}(\text{alanine})_2(\text{H}_2\text{O})$ (as discussed above) and for $\text{Cu}(\text{tartrate})(\text{H}_2\text{O})_3$ (see below). However, these changes are not observed

for the sharp DMF peaks (165 and 38 ppm) and the wide spinning sideband pattern of broad peaks centered at -78 ppm.

It should be noted here that comparison of the intensity of the single, sharp DMF peak at 38 ppm to the sum of the peaks comprising the sharp spinning sideband pattern centered at 228 ppm reveals that the sample of $\text{Cu}_3(\text{BTC})_2$ contains 0.47 DMF per BTC or about 10 wt % residual DMF. This value is comparable to that obtained from the complete dissolution of the $\text{Cu}_3(\text{BTC})_2$ (see Experimental Section) which yielded 0.32 DMF per BTC or 7.5 wt % DMF.

With regard to the indifferent behavior of DMF to high-power proton decoupling, it is obviously undergoing rapid motion and, as a result, is "self-decoupled" from any static dipolar interaction. As for the static species at -78 ppm, it is apparently sufficiently far and/or "paramagnetically-uncoupled" from the rigid-ring protons so that it experiences minimal ^{13}C - ^1H dipolar coupling antics (see below). Assignment of this resonance to the $\text{BTC}-\text{CO}_2^-$ group is consistent with its most-distal position relative to the ring-protons (and, hence, reduced static-dipolar interaction).

Considering the assignments of the remaining BTC-ring carbon peaks, they are not as straightforward as CO_2^- peak. Ishii et al.²⁶ employed ^{13}C - ^1H dipolar recoupling to obtain unambiguous assignments of the paramagnetically shifted peaks in $\text{Cu}(\text{alanine})_2(\text{H}_2\text{O})$. This method was also applied to $\text{Cu}_3(\text{BTC})_2$, where it was anticipated that ^{13}C - ^1H "dephasing"²⁶ would be most pronounced for the protonated ring-carbon; less so for its nonprotonated neighboring ring carbon; and least for the already-assigned CO_2^- group. These spectra, obtained with and without high-power proton decoupling, are shown in Figure 13. Solid $(\text{NH}_4)_3\text{BTC}$ was used as a diamagnetic control²⁶ for these experiments. The results show that the CO_2^- peak (-78 ppm) exhibits a dephasing ratio (S/S_0)²⁶ of 50%, which is close to the 44% value observed for this group in $(\text{NH}_4)_3\text{BTC}$, thus further affirming this assignment. However, the sharp peak at 228 ppm and broad peaks at 240 and 218 ppm exhibited quite similar ratios of 28% and 24%, respectively (Paramagnetic effects are assumed to be the cause of the virtually identical dephasing ratios of the protonated and nonprotonated ring carbons of $\text{Cu}_3(\text{BTC})_2$); therefore, the assignments are still not entirely clear. By comparison, the nonprotonated and protonated

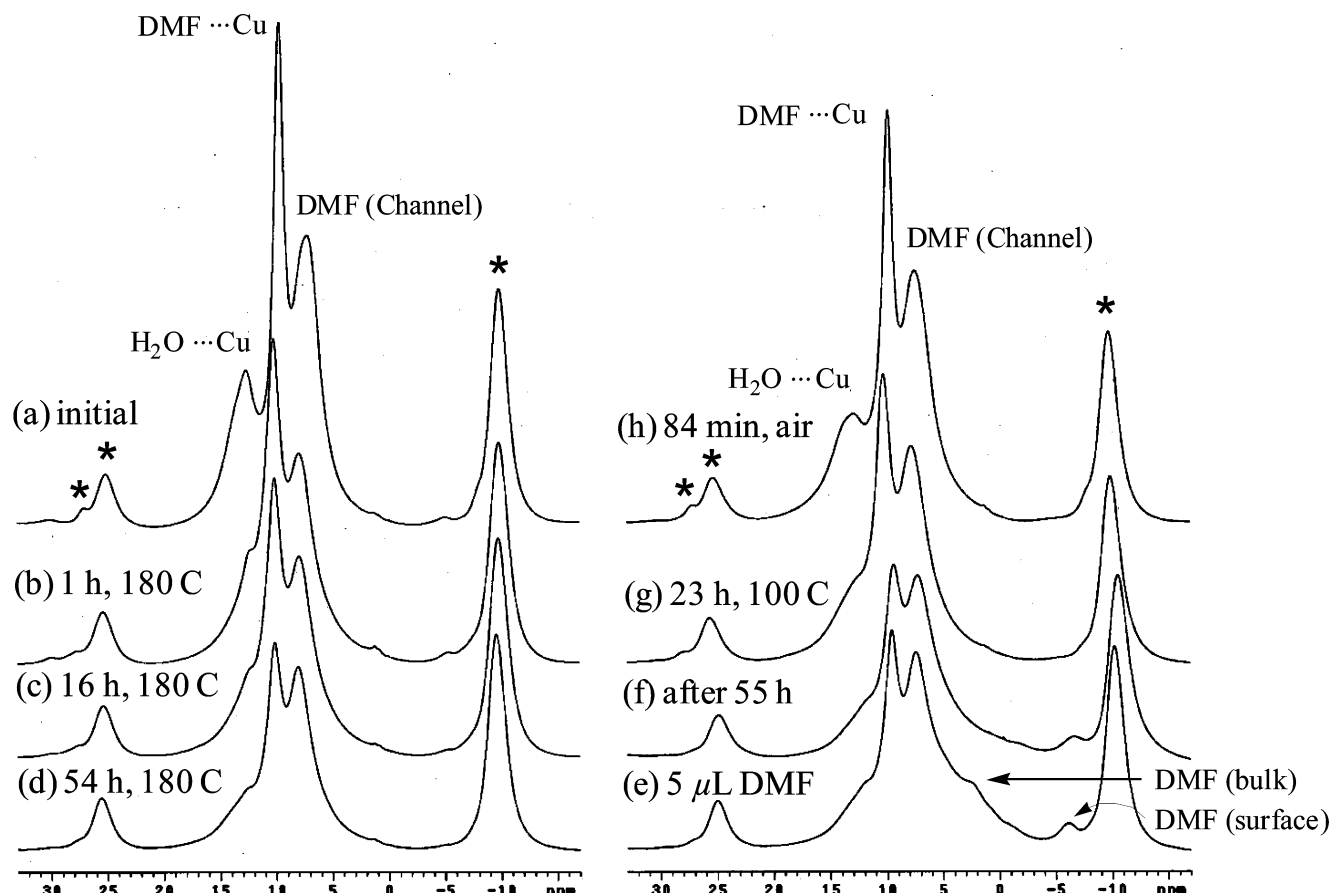


Figure 11. ¹H MAS NMR spectra (9.4 T) obtained for nominally dry Cu₃(BTC)₂: (a) initial spectrum; (b–d) after heating to 180 °C to drive off water and DMF; (e–f) after addition of 5 μ L of DMF; (g) after heating to 100 °C to readsorb DMF; and (h) after exposure to air to readsorb water. Spinning sidebands are marked by asterisks at the top of each stack.

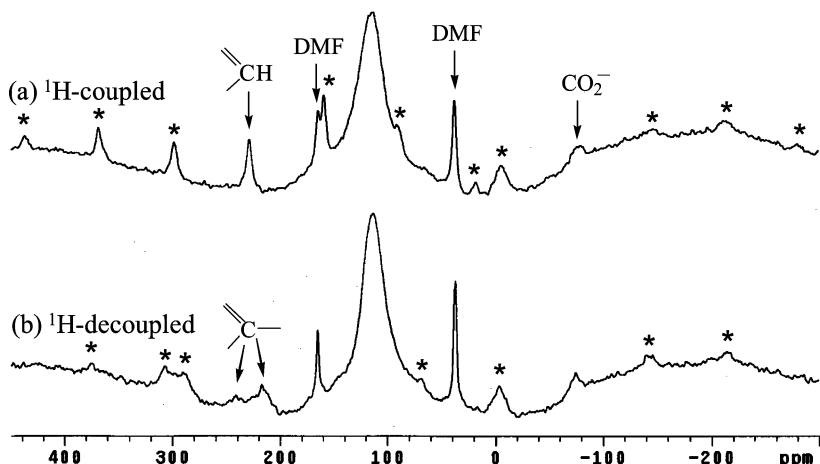


Figure 12. ¹³C MAS NMR spectra (9.4 T) obtained for nominally dry Cu₃(BTC)₂ without (a) and with (b) high-power proton decoupling. Assignments are indicated in the spectra (see text). Spinning sidebands (asterisks) and centerbands are indicated (see text).

ring carbons of (NH₄)₃BTC gave very discriminating dephasing ratios of 38% and 12%, respectively. Yet a tentative assignment of the sharp 228 ppm peak to the (methine) protonated-ring carbon is suggested by its very similar appearance to the sharp peaks detected for the methine carbons in Cu(tartrate)(H₂O)₃ (see below). Furthermore, in ¹³C CP-MAS NMR spectra recently obtained by Bertmer [Bertmer, M.; Poeppi, A.; Hartmann, M. Multinuclear Solid-State NMR on Metal-Organic Framework Materials (MOFs). Poster presented at 50th Experimental NMR Conference, Pacific Grove, CA, March 29–April 3, 2009] the sharp 228 ppm peak is the only carbon detected for

Cu₃(BTC)₂—an observation entirely consistent with its assignment to the CH group. The remaining assignment of the nonprotonated ring carbons falls to the broad peaks at 240 and 218 ppm. The presence of two peaks suggest inequivalent sites for this carbon; indeed, inspection of the crystal structure¹⁴ shows two sites adjacent to the channels whereas the third is distant, consistent with the approximate 2:1 ratio of the 240 and 218 ppm peaks. Finally, the fact that these peaks are not sufficiently decoupled by moderate-speed MAS alone may be due to the adjacent position of these carbons between two, otherwise paramagnetically isolated C–H (methane) spin pairs.

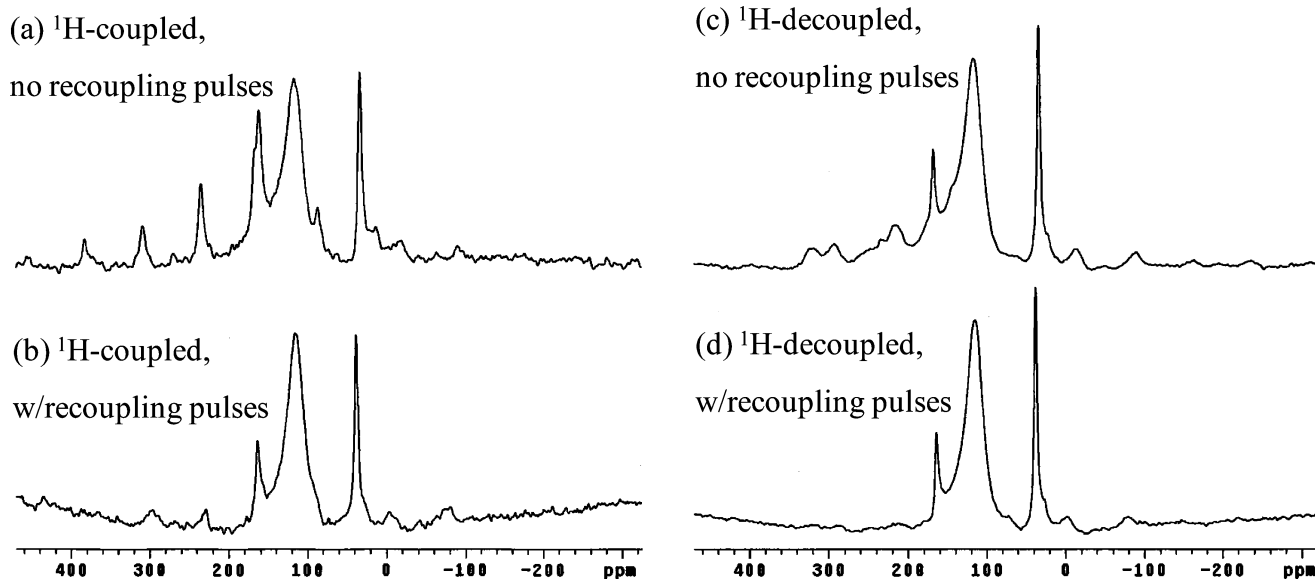


Figure 13. ^{13}C MAS NMR recoupling spectra (9.4 T, $\nu_R = 7000$ Hz) obtained for nominally dry $\text{Cu}_3(\text{BTC})_2$ without (a, b) and with (c, d) high-power proton decoupling (see text).

However, moderate-speed MAS is able to effectively narrow the more isolated (and separated) methine carbons.

The vanishing behavior of the sharp, MAS-decoupled peak at 228 ppm when high-power proton decoupling is applied is known to occur for $^{13}\text{C}-^1\text{H}$ dipolar interactions experiencing periodic effects such as molecular motion and/or spin-diffusion where maximum broadening is observed when the characteristic time of the decoupler field strength ($2\pi/\omega_1$) coincides with the correlation time (τ_c) of the modulation.³⁰ This behavior is indeed exhibited by the 228 ppm peak in spectra acquired under varied decoupling power (not shown). Thus, sufficient decoupler strength (ω_1) is not experimentally possible to reattain the line-narrowing condition $\omega_1\tau_c \gg 1$.³⁰

MAS NMR of Cu(II) Model Compounds. The negative paramagnetic-shifting (−78 ppm) of the CO_2^- group adjacent to Cu(II) in $\text{Cu}_3(\text{BTC})_2$ is in agreement with the negative shifts observed for groups adjacent to Cu(II) in $\text{Cu}(\text{alanine})_2(\text{H}_2\text{O})\text{:CO}_2^-$, −183 ppm; CH, −269 ppm (Table 5).²⁶ Moreover, the positive paramagnetic-shifting of the peaks for the BTC-ring carbons more distant from the Cu(II) (240, 228, and 218 ppm) is consistent with the 173 ppm shift of the Cu(II)-removed CH_3 in $\text{Cu}(\text{alanine})_2(\text{H}_2\text{O})$. However, the other model compounds provide mixed results.

For example, consider the ^{13}C MAS NMR spectrum obtained for $\text{Cu}(\text{tartrate})(\text{H}_2\text{O})_3$, with and without high-power proton decoupling, shown in the bottom two spectra of Figure 14. ^1H MAS NMR spectra (not shown) yield two broad, equal-intensity, overlapping sideband patterns centered at about 6 and 4 ppm which, judging by the rather sharp ^{13}C MAS NMR spectra for the methine carbons (indicative of paramagnetically isolated C–H spin systems, see above), are assignable to the two different methine protons,³¹ Figure 8. In the ^{13}C MAS NMR spectra, there are four different spinning sideband patterns, two of which are quite sharp (one in the presence of decoupling) and two of which are broad. The broadened sideband patterns are attributed to the two types of CO_2^- groups present in crystal structures of both the *meso*- and *d*-tartrate Cu(II) compounds³¹ (Figure 8), which are presumably also present in the $\text{Cu}(\text{L-tartrate})(\text{H}_2\text{O})_3$ model compound. The negatively shifted set at −427 ppm is assigned to $\text{Cu}-\text{CO}_2^--\text{H}_2\text{O}$ by analogy to the negative shift exhibited by the singly Cu(II)-coordinated CO_2^-

group in $\text{Cu}(\text{alanine})_2(\text{H}_2\text{O})^{26}$ (−183 ppm, Table 5). The positively shifted set at 483 ppm is then assigned to $\text{Cu}-\text{CO}_2^--\text{Cu}$ group. The shift assigned for the doubly Cu(II)-coordinated CO_2^- is quite close to the 501 ppm shift observed for the triply bridging CO_3^{2-} group^{32,33} in $\text{Cu}(\text{CO}_3)\text{Cu}(\text{OH})_2$ (top spectrum, Figure 14). The remaining sharp resonances for the two types³¹ of methines, which are quite identical in appearance to the sharp peak assigned to the methine in $\text{Cu}_3(\text{BTC})_2$ (see above), are tentatively assigned on the basis of their proximity to the singly Cu(II)-coordinated and doubly Cu(II)-coordinated CO_2^- groups, with the positively shifted methine (171 ppm) assumed to be adjacent to the positively shifted CO_2^- (483 ppm) and the slightly negatively shifted methine (−35 ppm) adjacent to the negatively shifted CO_2^- (−427 ppm). Also, as discussed above for $\text{Cu}_3(\text{BTC})_2$, the methine carbon at −35 ppm undergoes broadening under high-power proton decoupling whereas the methine at 171 ppm and both CO_2^- groups do not. This behavior is further evidence that the assignment of the −35 ppm methine is correct as this group is most-distant from the Cu(II) centers and would tend to experience reduced electron spin-diffusion “decoupling” effects.

Finally, Cu(II) dimer compounds are of interest owing to their antiferromagnetic behavior,^{34–36} i.e., they exhibit decreasing magnetic susceptibility with decreasing temperature leading to the complete disappearance of paramagnetism/magnetic susceptibility at sufficiently low temperatures. Indeed, Oldfield et al.²⁹ only observed measurable ^{13}C MAS NMR signals for $\text{Cu}(\text{formate})_2(\text{C}_5\text{H}_5\text{N})$ at low temperatures, where the shift observed for the CO_2^- group at 163 ppm at 92 K is practically unshifted with respect to typical carboxylate groups in diamagnetic compounds (below 120 K only residual paramagnetism has been observed³⁶). At higher temperatures, however, Oldfield et al.²⁹ observed broadening and upfield-shifting (negative) of the carboxylate peak until the signal was too broad to observe near 173 K, owing to the onset of paramagnetic behavior.

Attempts at obtaining ^{13}C MAS NMR spectra of the cuprate dimer $\text{Cu}(\text{acetate})_2(\text{H}_2\text{O})$,³⁷ which yielded a single, broad ^1H MAS NMR sideband pattern centered at 15 ppm, were unsuccessful, even at temperatures down to 173 K. The susceptibility of the acetate complex only becomes small below about 100 K³⁵ (attaining zero-susceptibility below 50 K³⁴). Thus, lower

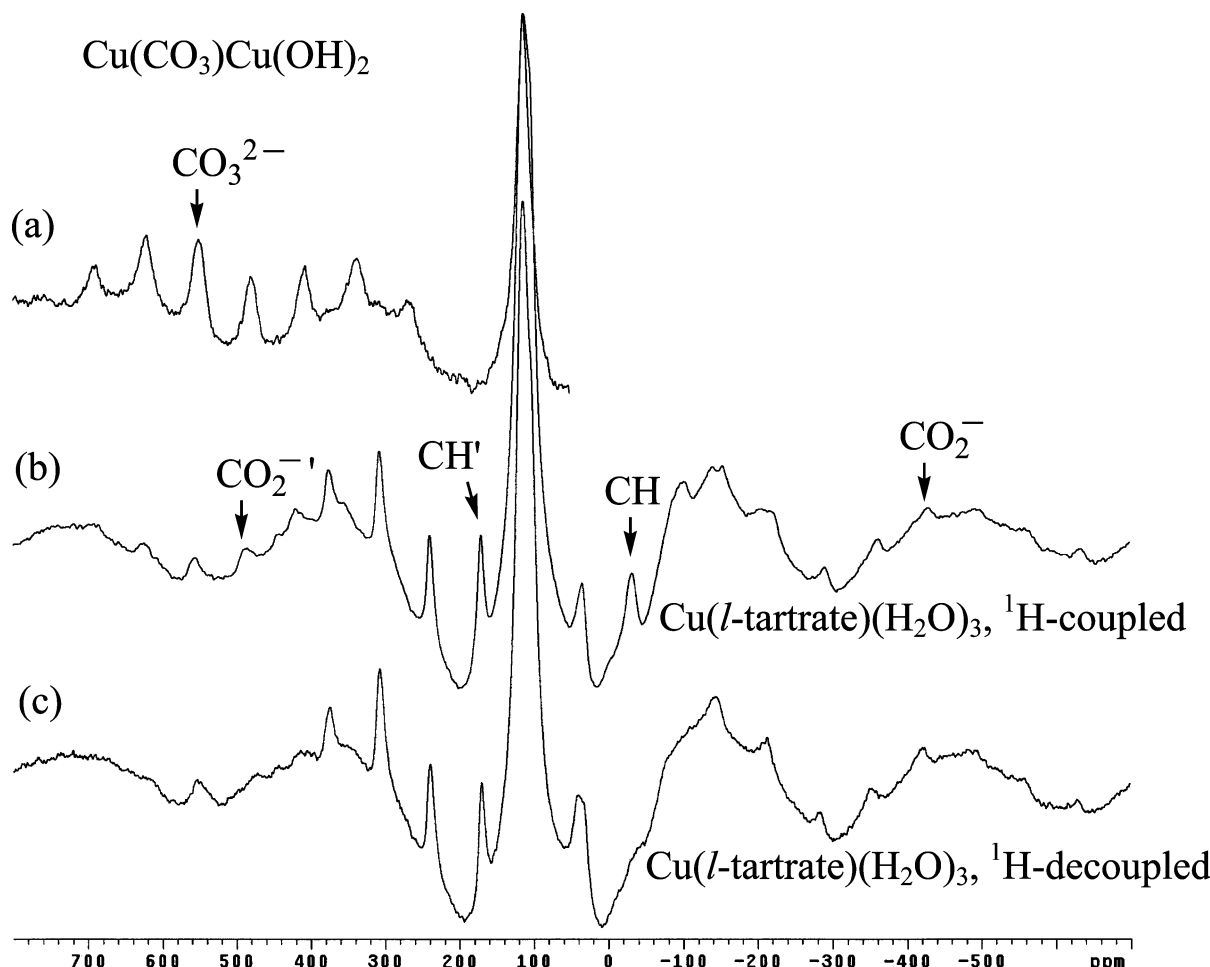


Figure 14. ^{13}C MAS NMR spectra (9.4 T) obtained for $\text{Cu}(\text{CO}_3)\text{Cu}(\text{OH})_2$ (no decoupling), (a) and $\text{Cu}(l\text{-tartrate})(\text{H}_2\text{O})_3$, without (b) and with (c) high-power proton decoupling. Centerbands of various spinning sideband patterns are indicated (see text).

temperatures are required to observe ^{13}C MAS NMR spectra of $\text{Cu}(\text{acetate})_2(\text{H}_2\text{O})$ than our current instrumentation allows (133 K). With regard to $\text{Cu}_3(\text{BTC})_2$, Williams et al.³⁸ have shown that its susceptibility is greatly reduced at room temperature relative to the formate and acetate compounds, which they surmise is due to weak ferromagnetic coupling between different Cu(II)–Cu(II) dimers as a result of the polymeric nature of this compound (in contrast to the discrete, molecular structures of other dimer compounds). Thus, it is evidently the polymeric nature of $\text{Cu}_3(\text{BTC})_2$ which permits the observation of its ^{13}C MAS NMR spectrum at room temperature.

MAS NMR of Cu₃(BTC)₂ Interaction with NH₃. Kaskel et al.²⁸ previously noted that gaseous NH₃ adsorption causes irreversible changes to $\text{Cu}_3(\text{BTC})_2$ but did not elaborate on the nature of the resulting material. Moreover, Yaghi et al.¹¹ concluded NH₃ had undergone chemisorption with $\text{Cu}_3(\text{BTC})_2$ owing to its irreversible color change from violet to light blue. Thus, MAS NMR was employed to characterize the reaction between $\text{Cu}_3(\text{BTC})_2$ and NH₃.

^1H MAS NMR spectra obtained following exposure of $\text{Cu}_3(\text{BTC})_2$ to NH₃, under both dry and humid (80% R.H.) conditions, are shown in Figure 15. The simple observation that, following both treatments, the simple, elegant, sharp spinning sideband pattern of the BTC-ring protons is drastically altered demonstrates that the basic structure has undergone dramatic change. Additionally, new features are consistent with the reactions presented above (Scheme 2).

For example, under dry conditions (Figure 15a), the sharp Cu_3BTC_2 sideband pattern is replaced by two, broad spinning

sideband patterns, one paramagnetically shifted to -133 ppm and the other centered near the normal, (unparamagnetically shifted) range. Also evident are two sharp peaks lacking spinning sidebands at 3.1 and ca. 0 ppm which are attributed to residual DMF and a background impurity present in the empty stator (presumably silicon grease), respectively. For the methine protons of BTC, disruption of the paramagnetically induced “uncoupling” of the methine protons has occurred, restoring the normal, static dipolar interaction typical of a diamagnetic species; thus, the extremely broad sideband pattern centered near 0 ppm is attributed to a BTC species which is less associated with the Cu(II) centers and experiencing its normal, strong dipolar ^1H – ^1H coupling. Although diminished in breadth, the -133 ppm sideband pattern is quite similar to that of $\text{Cu}(\text{CO}_3)\text{Cu}(\text{OH})_2$ (Figure 15d) and is thus assigned to a $\text{Cu}(\text{OH})_2$ species, the slight formation of which evidently occurred during handling of the sample in (moist) air. However, noticeably absent are signals for the anticipated (Scheme 2) diammine copper(II) complex. Saito and Kanda³⁹ observed ^1H NMR resonances for both NH₃ and H₂O in $\text{Cu}(\text{NH}_3)_4\text{SO}_4 \cdot \text{H}_2\text{O}$ at liquid helium temperatures, but the prospect of obtaining spectra at higher temperatures was not discussed. An exhaustive literature search failed to find any other ^1H NMR studies of solid ammonia–copper(II) complexes. Therefore, it is likely that, owing to an unfavorable paramagnetic interaction with Cu(II), protons in the presumed ammonia–copper(II) complex present in the sample are not observable at room temperature (low temperature spectra were not investigated).

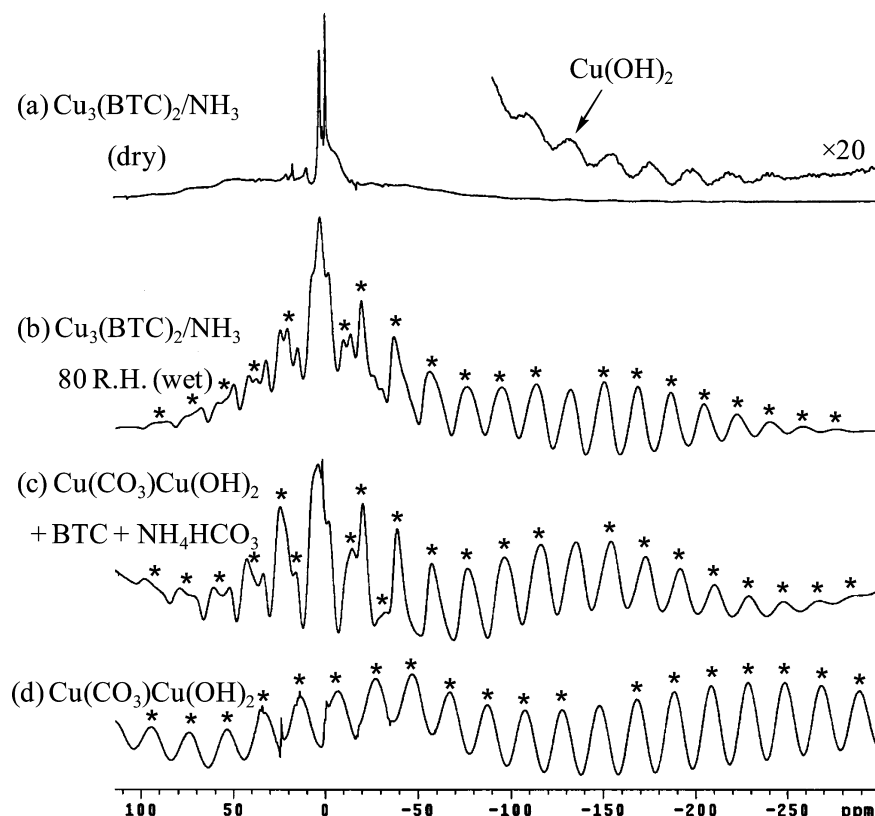


Figure 15. ^1H MAS NMR spectra obtained for $\text{Cu}_3(\text{BTC})_2$ exposed to NH_3 under (a) dry (9.4 T, $\nu_{\text{R}} = 7000$ Hz) and (b) humid (80% R.H., 14 T, $\nu_{\text{R}} = 10\,000$ Hz) conditions. Spectrum (c) (9.4 T, $\nu_{\text{R}} = 7000$ Hz) was obtained from the reaction of BTC with $\text{Cu}(\text{CO}_3)\text{Cu}(\text{OH})_2$ and NH_4HCO_3 (see text). The spectrum of $\text{Cu}(\text{CO}_3)\text{Cu}(\text{OH})_2$ (9.4 T, $\nu_{\text{R}} = 7000$ Hz) is shown in (d). Spinning sidebands are marked by asterisks in the lower spectra. Enhanced inset in spectrum (a) shows centerband for $\text{Cu}(\text{OH})_2$ species (see text).

Under humid conditions (Figure 15b) the -133 ppm sideband pattern for the $\text{Cu}(\text{OH})_2$ species is more intense and its individual peaks are sharper; thus, NH_3 exposure, in the presence of water, is able to effect the expected conversion of Cu_3BTC_2 to $\text{Cu}(\text{OH})_2$ (Scheme 2). The sideband pattern centered near 0 ppm is also sharper, perhaps owing to increased motion and/or solvation by water. Multiple peaks are also evident in the sideband patterns near zero which are assigned to the anticipated $(\text{NH}_4)_3\text{BTC}$ product (Scheme 2). Further, note that residual water and/or DMF peaks are broadened (compared to the corresponding signals in the dry-reacted material), apparently owing to contact with solvated Cu^{2+} . As discussed above for the case of the dry material, no peaks attributable to possible ammonia–copper(II) complexes are observed.

Finally, as shown in Figure 15c, features of the two primary spinning sidebands observed in Figure 15b for NH_3 -exposed Cu_3BTC_2 under humid conditions are faithfully reproduced by the reaction of BTC with $\text{Cu}(\text{CO}_3)\text{Cu}(\text{OH})_2$ and NH_4HCO_3 in water (followed by drying), yielding an authentic mixture of the $\text{Cu}(\text{OH})_2$ and $(\text{NH}_4)_3\text{BTC}$ products.

Conclusions

The MOF $\text{Cu}_3(\text{BTC})_2$ reacts with ammonia to form a presumed diammine–copper(II) complex under dry conditions and, under humid conditions, a $\text{Cu}(\text{OH})_2$ species and $(\text{NH}_4)_3\text{BTC}$; thus suffering an irreversible loss of structure and porosity. Initial removal capacities were on the order of 6–9 mol/kg at saturation, among the highest dynamic loadings for ammonia-removal sorbents; however, breakthrough testing of exhausted samples reflects the significant decrease in available reactive sites and capacity. Nitrogen adsorption, PXRD, and

NMR testing of fresh and exhausted samples all provide evidence for the permanent loss of structure and/or porosity, with samples challenged with ammonia under humid conditions undergoing the largest change. Although the porosity of the material is destroyed, the resulting capacity of the exhausted samples for ammonia is indicative of an extended reactive network consistent with that of the copper(II) complex products. Though antiferromagnetic, ^1H and ^{13}C MAS NMR spectra of Cu_3BTC_2 are observable at room temperature and its paramagnetically shifted resonances have been assigned. That the ^{13}C MAS NMR spectrum of Cu_3BTC_2 is observable at room temperature is consistent with its greatly reduced susceptibility at room temperature compared to other Cu(II)–Cu(II) dimers.

Acknowledgment. The authors thank David Britt and Dr. Omar Yaghi of the University of California, Los Angeles, for synthesizing the $\text{Cu}_3(\text{BTC})_2$ and providing PXRD data on fresh and exhausted materials and Dr. Marko Bertmer, Universitaet Leipzig, for helpful discussions regarding ^{13}C CP-MAS NMR studies of this compound. This work was completed under Joint Science and Technology Office for Chemical and Biological Defense (JSTO–CBD) Project No. BA07PRO104. Work performed on the high-field (17.5 T) NMR system at New York Structural Biology Center was supported under U.S. Department of Defense Contract W911NF0710053. NYSBC is a STAR center supported by the New York State Office of Science, Technology, and Academic Research. NMR Resources supported by NIH P41 GM66354.

Supporting Information Available: Raw nitrogen isotherm data for fresh and ammonia-exhausted samples, ^1H and ^{13}C MAS NMR spectra for solvent extracted $\text{Cu}_3(\text{BTC})_2$ and $(\text{NH}_4)_3\text{BTC}$,

the MAS NMR ¹³C–¹H dipolar recoupling sequence, and XRD patterns of fresh and exposed Cu₃(BTC)₂ compared to Mercury simulations. This material is available free of charge via the Internet at <http://pubs.acs.org>.

Note Added after ASAP Publication. This manuscript was originally published ASAP July 1, 2009. Due to a production error the copyright line was incorrect. The corrected version was reposted on July 10, 2009.

References and Notes

- (1) Petit, C.; Karwacki, C.; Peterson, G.; Bandosz, T. J. *J. Phys. Chem. C* **2007**, *111*, 12705–12714.
- (2) Petit, C.; Bandosz, T. J. *J. Phys. Chem. C* **2007**, *111*, 16445–16452.
- (3) Yaghi, O. M.; Li, H.; Davis, C.; Richardson, D.; Groy, T. *Acc. Chem. Res.* **1998**, *31*, 474–484.
- (4) Barton, T. J.; Bull, L. M.; Klemperer, W. G.; Loy, D. A.; McEnaney, B.; Misono, M.; Monson, P. A.; Pez, G.; Scherer, G. W.; Vartuli, J. C.; Yaghi, O. M. *Chem. Mater.* **1999**, *11*, 2633–2656.
- (5) O’Keeffe, M.; Eddaoudi, M.; Li, H.; Reineke, T.; Yaghi, O. M. *J. Solid State Chem.* **2000**, *152*, 3–20.
- (6) Braun, M. E.; Steffek, C. D.; Kim, J.; Rasmussen, P. G.; Yaghi, O. M. *Chem. Commun.* **2001**, 2532–2533.
- (7) Eddaoudi, M.; Li, H.; Yaghi, O. M. *J. Am. Chem. Soc.* **2000**, *122*, 1391–1397.
- (8) Rowsell, J. L. C.; Millward, A. R.; Park, K. S.; Yaghi, O. M. *J. Am. Chem. Soc.* **2004**, *126*, 5666–5667.
- (9) Chen, B.; Ockwig, N. W.; Millward, A. R.; Contreras, D. S.; Yaghi, O. M. *Angew. Chem., Int. Ed.* **2005**, *30*, 4745–4749.
- (10) Walton, K. S.; Millward, A. R.; Dubbeldam, D.; Frost, H.; Low, J. J.; Yaghi, O. M.; Snurr, R. Q. *J. Am. Chem. Soc.* **2008**, *130*, 406–407.
- (11) Britt, D.; Tranchemontagne, D.; Yahgi, O. *Proc. Natl. Acad. Sci. U.S.A.* **2008**, *105*, 11623–11627.
- (12) Dathe, H.; Peringer, E.; Roberts, V.; Jentys, A.; Lercher, J. A. *C. R. Chim.* **2005**, *8* (3–4), 753–763.
- (13) Dathe, Hendrik; Jentys, Andreas; Lercher, Johannes, A. *Phys. Chem. Chem. Phys.* **2005**, *7* (6), 1283–1292.
- (14) Chui, S. S. Y.; Lo, S. M. F.; Charmant, J. P. H.; Orpen, A. G.; Williams, I. D. *Science* **1999**, *283*, 1148–1150.
- (15) Vishnyakov, A.; Ravikovich, P. I.; Neimark, A. V.; Bulow, M.; Wang, Q. M. *Nano Lett.* **2003**, *3*, 713–718.
- (16) Vitillo, J. G.; Regli, L.; Chavan, S.; Ricchiardi, G.; Spoto, G.; Dietzel, P. D. C.; Bordiga, S.; Zecchina, A. *J. Am. Chem. Soc.* **2008**, *130*, 8386–8396.
- (17) Margerum, D. W.; Rosen, H. M. *J. Am. Chem. Soc.* **1967**, *89*, 1088–1092.
- (18) Martini, G.; Bassetti, V. *J. Phys. Chem.* **1979**, *83*, 2511–2515.
- (19) Massey, A. G. In *Comprehensive Inorganic Chemistry*, 1st ed.; Trotman-Dickenson, A. F., Editor; Pergamon Press, Ltd.: Oxford, UK, 1973.
- (20) March, J. *Advanced Organic Chemistry: Reactions, Mechanisms, and Structure*, 2nd ed.; McGraw-Hill: New York, 1977.
- (21) Chen, B.; Eddaoudi, M.; Reineke, T. M.; Kampf, J. W.; O’Keeffe, M.; Yaghi, O. M. *J. Am. Chem. Soc.* **2000**, *122*, 11559–11560.
- (22) Chen, B.; Ockwig, N. W.; Millward, A. R.; Contreras, D. S.; Yaghi, O. M. *Angew. Chem., Int. Ed.* **2005**, *44*, 4745–4749.
- (23) Yang, Q.; Zhong, C. *J. Phys. Chem. B* **2006**, *110*, 655–658.
- (24) Rowsell, J. L. C.; Yaghi, O. M. *J. Am. Chem. Soc.* **2006**, *128*, 1304–1315.
- (25) Meyer, M. H.; Singh, P.; Hatfield, W. E.; Hodgson, D. J. *Acta Crystallogr. B* **1972**, *28*, 1607–1613.
- (26) Ishii, Y.; Wickramasinghe, N. P.; Chimon, S. *J. Am. Chem. Soc.* **2003**, *125*, 3438–3439.
- (27) Liu, K.; Ryan, D.; Koji, N.; McDermott, A. *J. Am. Chem. Soc.* **1995**, *117*, 6897–6906.
- (28) Schlichte, K.; Kratzke, T.; Kaskel, S. *Microporous Mesoporous Mater.* **2004**, *73*, 81–88.
- (29) Walter, T. H.; Oldfield, E. *J. Chem. Soc., Chem. Commun.* **1987**, 646–647.
- (30) (a) Maricq, M. M.; Waugh, J. S. *J. Chem. Phys.* **1979**, *70*, 3300–3316. (b) Rothwell, W. P.; Waugh, J. S. *J. Chem. Phys.* **1981**, *74*, 2721–2732.
- (31) Prout, C. K.; Carruthers, J. R.; Rossotti, F. J. C. *J. Chem. Soc. A* **1971**, 3336–3342.
- (32) Eby, R. K.; Hawthorne, F. C. *Acta Crystallogr. B* **1993**, *49*, 28–56.
- (33) Zigan, F.; Joswig, W.; Schuster, H. D. *Z. Kristallogr.* **1977**, *145*, 412–426.
- (34) Hay, P. J.; Thibeault, J. C.; Hoffman, R. *J. Am. Chem. Soc.* **1975**, *97*, 4884–4899.
- (35) Figgis, B. N.; Martin, R. L. *J. Chem. Soc.* **1956**, 3837–3846.
- (36) Martin, R. L.; Waterman, H. *J. Chem. Soc.* **1959**, 2960–2968.
- (37) Van Niekerk, J. N.; Schoening, F. R. L. *Acta Crystallogr.* **1953**, *6*, 227–232.
- (38) Zhang, X. X.; Chui, S. S.-Y.; Williams, I. D. *J. Appl. Phys.* **2000**, *87*, 6007–6009.
- (39) Saito, S.; Kanda, E. *J. Phys. Soc. Jpn.* **1967**, *22*, 1241–1245.

JP902736Z